



OPEN

Significantly improving zero-shot X-ray pathology classification via fine-tuning pre-trained image-text encoders

Jongseong Jang^{1,3}, Daeun Kyung^{2,3}, Seung Hwan Kim¹, Honglak Lee¹, Kyunghoon Bae¹ & Edward Choi²✉

Deep neural networks are increasingly used in medical imaging for tasks such as pathological classification, but they face challenges due to the scarcity of high-quality, expert-labeled training data. Recent efforts have utilized pre-trained contrastive image-text models like CLIP, adapting them for medical use by fine-tuning the model with chest X-ray images and corresponding reports for zero-shot pathology classification, thus eliminating the need for pathology-specific annotations. However, most studies continue to use the same contrastive learning objectives as in the general domain, overlooking the multi-labeled nature of medical image-report pairs. In this paper, we propose a new fine-tuning strategy that includes positive-pair loss relaxation and random sentence sampling. We aim to improve the performance of zero-shot pathology classification without relying on external knowledge. Our method can be applied to any pre-trained contrastive image-text encoder and easily transferred to out-of-domain datasets without further training, as it does not use external data. Our approach consistently improves overall zero-shot pathology classification across four chest X-ray datasets and three pre-trained models, with an average macro AUROC increase of 4.3%. Additionally, our method outperforms the state-of-the-art and marginally surpasses board-certified radiologists in zero-shot classification for the five competition pathologies in the CheXpert dataset.

The success of deep neural networks (DNNs) for visual and textual data led to their wide adoption in diverse domains and tasks, including pathology classification based on medical images. Although there have been some successful applications of neural networks to medical images, such as diabetic retinopathy classification^{1,2} and skin cancer detection³, their widespread adoption has been hindered due to the need for large amounts of high-quality training samples. This poses a great challenge especially in the medical imaging domain, as qualified experts are required to create labeled samples, not to mention the difficulty of collecting images to begin with as they require special machinery. Recent studies tackled this problem with some success by leveraging advantage of the powerful pre-trained models trained on large-scale general domain data. Some demonstrated that fine-tuning a pre-trained image encoder in a supervised manner can yield impressive performance^{4–6}. However, this approach still requires a certain amount of expert-annotated images. To mitigate this dependency, researchers are exploring medical image-text representation learning^{7–10}, inspired by large-scale image-text pre-training models like CLIP¹¹. For instance, ConViRT⁷ introduces contrastive learning to the medical domain, GloRia⁸ aims to align image and text embeddings both globally and locally. BioViL⁹ incorporates temporal content by accounting for prior images and reports. CheXzero¹⁰, closely related to our approach, demonstrates that effective pathology classification can be achieved without an expert-annotated training set by aligning X-ray images with reports from the MIMIC-CXR dataset, in the same manner as CLIP.

However, the models often fail to properly address the false-negative case, i.e., image-report pairs with the same label from different patients. This issue becomes evident when considering the medical image-report pairs with their multi-labeled nature. For example, let us imagine two chest X-ray studies where one has Lung Opacity, Edema, Pneumonia, Support Devices, and the other has the first two. Ideally, their reports should share the semantics of Lung Opacity and Edema (Fig. 1). However, most of medical contrastive learning methods may inaccurately categorize these partially overlapping pairs as entirely distinct, leading to sub-optimal representation learning. While MedCLIP¹² attempts to address this using CheXpert¹³ labels, it is constrained by the labeler's

¹LG AI Research, 07796 Seoul, Republic of Korea. ²KAIST, Kim Jaechul Graduate School of AI, 34141 Daejeon, Republic of Korea. ³These authors contributed equally to this work. ✉email: edwardchoi@kaist.ac.kr

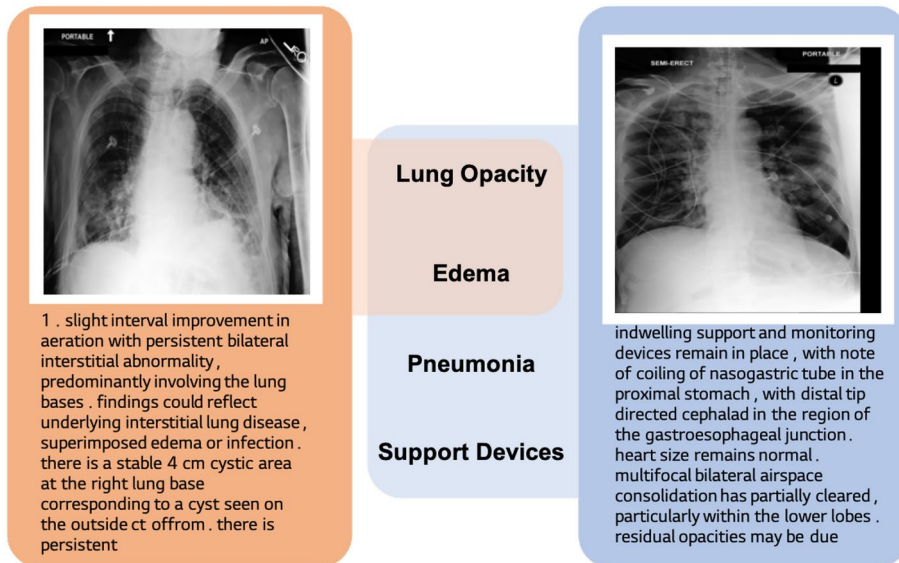


Figure 1. Example of false-negatives between medical data. Two image-text pairs share two classes of disease; lung opacity and edema. Existing image-text contrastive learning frameworks deal other pair as perfectly negative one.

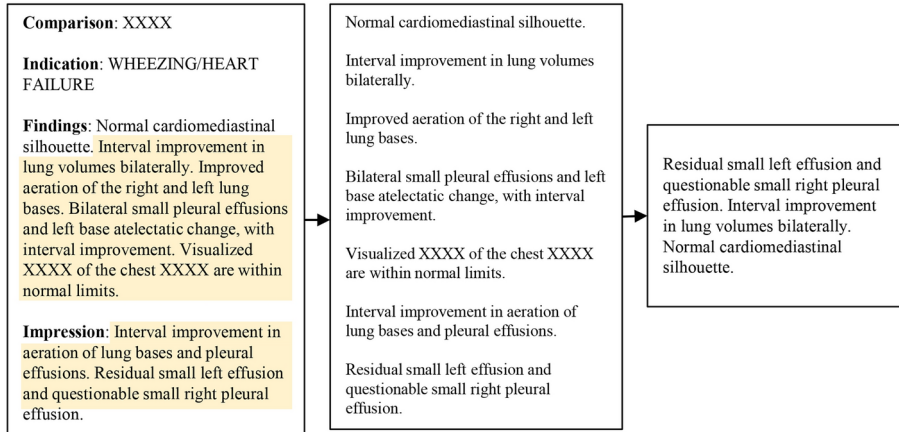


Figure 2. Example of random text sampling. Given the original free-form report (left), we extract only the “Findings” and “Impression” section and split them into sentences (middle). n sentences are randomly selected to make new positive text pairs (right).

limitations and the predefined disease classes. Our method employs loss relaxation, which clips the loss based on similarity between the target sample, thus avoiding reliance on expert labels.

On the other hand, we propose a new text processing method for medical report to improve the contrastive learning performance. In the medical domain, text augmentation techniques, such as random insertion, deletion, or backtranslation¹⁴ are typically avoided due to the high risk of information loss, as medical reports are often brief and dense with critical information. Previous method¹⁵ involves substituting medical concepts with the corresponding terms of the Unified Medical Language System (UMLS), require both powerful extraction tools and extensive medical knowledge. In contrast, our approach utilizes a straightforward yet effective technique: sentence-level random selection that preserves the content of each sentence as it is, without additional knowledge.

In this work, we propose a new fine-tuning strategy for zero-shot pathology classification by taking into account the multi-label nature of medical image-text pairs. Our method consists of sentence sampling and loss relaxation, which are based on two core observations: (1) Every sentence in a report contains important clinical information; (2) There are many false-negative pairs, but practically no perfectly positive pairs. Our label-free method can be applied to any pre-trained contrastive image-text encoders to enhance downstream zero-shot performance. This fine-tuning strategy consistently improved zero-shot pathology classification when applied to three pre-trained models on four different chest X-ray datasets, even surpassing board-certified radiologists in some instances.

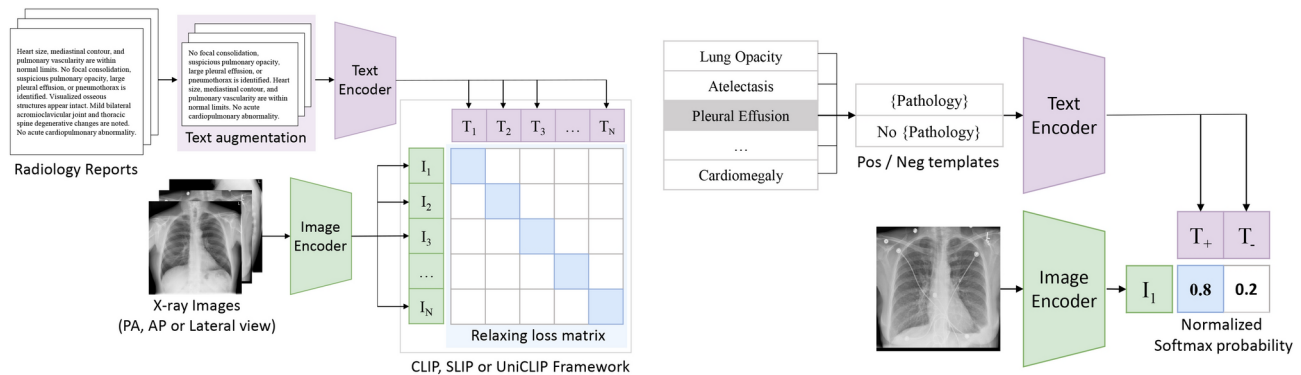


Figure 3. (left) Training phase. Our fine-tuning strategies, random text sampling and relaxation loss, on contrastive learning frameworks with a medical multi-modal dataset. Our proposed methods could be easily applied to various image-text contrastive learning frameworks, such as CLIP, SLIP, and UniCLIP. (right) Inference phase. For the zero-shot pathology classification task, the text encoder works as a multi-label classifier by embedding the names or descriptions of the pathologies in the target dataset at test time.

	CheXpert		Open-i		PadChest		VinDr-CXR	
	Avg. 5 AUC	Avg. total AUC	Avg. 5 AUC	Avg. total AUC	Avg. total AUC	Avg. total AUC	Avg. total AUC	Avg. total AUC
CLIP	0.870 \pm 0.006	0.771 \pm 0.001	0.785 \pm 0.030	0.691 \pm 0.010	0.685 \pm 0.026	0.801 \pm 0.020		
CLIP w/ ours	0.885 \pm 0.007	0.789 \pm 0.017	0.808 \pm 0.008	0.708 \pm 0.013	0.725 \pm 0.014	0.842 \pm 0.007		
SLIP	0.831 \pm 0.008	0.722 \pm 0.008	0.760 \pm 0.008	0.666 \pm 0.004	0.684 \pm 0.004	0.799 \pm 0.018		
SLIP w/ ours	0.884 \pm 0.009	0.779 \pm 0.020	0.810 \pm 0.016	0.719 \pm 0.018	0.741 \pm 0.005	0.831 \pm 0.009		
UniCLIP	0.851 \pm 0.008	0.741 \pm 0.037	0.744 \pm 0.032	0.643 \pm 0.027	0.684 \pm 0.009	0.759 \pm 0.019		
UniCLIP w/ ours	0.888 \pm 0.006	0.802 \pm 0.018	0.788 \pm 0.016	0.694 \pm 0.006	0.717 \pm 0.011	0.843 \pm 0.016		

Table 1. The zero-shot classification performance of three different CLIP-based frameworks across four distinct datasets is provided (mean \pm std). The term 'w/ ours' refers to models that have been fine-tuned with our strategy, including random sentence sampling and loss relaxation. **Bold** means the best performance within each framework. For the CheXpert and Open-i datasets, we report the average AUC of 5 CheXpert competition pathologies and a total of 13 pathologies, respectively. For the PadChest and VinDr-CXR datasets, the average of 61 pathologies (where each has more than 100 samples) and 20 pathologies (where each has more than 20 samples), respectively.

The contribution of this work is summarized below:

- We propose a new fine-tuning strategy, random sentence sampling and loss relaxation, for zero-shot pathology classification from unlabeled X-ray images. Our methods can be applied easily across various pre-trained contrastive image-text encoders without the need for external knowledge or architectural modifications.
- We demonstrate that our proposed method consistently improves zero-shot pathology classification performance across four different chest X-ray datasets and three distinct pre-trained models. Notably, for the CheXpert dataset, our method sometimes outperforms board-certified radiologists in detecting five key diseases.
- Our fine-tuning strategy also showed consistent performance improvement for image-text alignment. Ablation studies were conducted simultaneously to verify the effectiveness of the proposed fine-tuning method.

Methods and materials

Zero-shot X-ray pathology classification

In this paper, we focus on the zero-shot X-ray pathology classification task following CheXzero¹⁰. Zero-shot evaluation refers to the process of training or fine-tuning a model on a large-scale dataset and then testing its performance on different datasets without further fine-tuning, known as cross-dataset zero-shot evaluation^{11,16}. We specifically address this challenge within the medical domain, using chest X-ray (CXR) images and their corresponding report. To achieve this, we first jointly train an image encoder E_{img} and a text encoder E_{txt} to predict the correct image-text pairs through InfoNCE loss (Fig. 3 (left)). Notably, we do not use manual labels for X-ray images during training. For the inference phase, we use the similarity between the image embedding of the target unseen X-ray image $I_{trg} \in \mathbb{R}^{H \times W \times 3}$ and the text embedding of the prompts T_c for target pathology c to conduct the zero-shot classification. We construct positive and negative prompts, $T_{+,c}$ and $T_{-,c}$, for each pathology c . We use the prompts of “{label}” and “no {label}” following Tiu et al.¹⁰ (e.g., “Atelectasis” and “No atelectasis”). Then we calculate the softmax probabilities for each pathology based on the cosine similarity between the embedding of the target image $E_{img}(I_{trg}) \in \mathbb{R}^{d_I}$ and the embedding of the positive/negative prompt

	mean AUC	Mean F1	Mean MCC
Radiologists (mean) ¹⁰	-	0.619	0.530
CLIP	0.870	0.578	0.423
CLIP w/ ours	0.885	0.603	0.443
CLIP _{ensemble}	0.887	0.613	0.519
CLIP _{ensemble} w/ ours	0.893	0.614	0.525
SLIP	0.831	0.578	0.423
SLIP w/ ours	0.884	0.608	0.424
SLIP _{ensemble}	0.845	0.564	0.456
SLIP _{ensemble} w/ ours	<u>0.893</u>	0.625	<u>0.537</u>
UniCLIP	0.851	0.561	0.458
UniCLIP w/ ours	0.888	0.610	0.522
UniCLIP _{ensemble}	0.881	0.614	0.524
UniCLIP _{ensemble} w/ ours	0.900	<u>0.623</u>	0.544

Table 2. Comparison with the performance of three board-certified radiologists on the CheXpert test dataset. We also compare the ensemble over the best model checkpoints from 3 runs with a different random seed. We report the average results across the five CheXpert competition pathologies. The mean AUC of radiologists is not available, as radiologist predictions are only binary. The colored cell means that the model outperformed the prediction performance of the expert radiologist. The best performance is in bold, and the second best is in underlined.

Testset	# of label	Metric	BioViL-T	CheXzero	Our _{single,best}
CheXpert	5	AUC	0.812	0.844 ± 0.008	0.884 ± 0.009
		F1	0.544	0.559 ± 0.005	0.608 ± 0.018
		MCC	0.361	0.417 ± 0.017	0.424 ± 0.035
	13	AUC	0.779	0.733 ± 0.008	0.779 ± 0.020
Open-i	5	AUC	0.785	0.771 ± 0.006	0.810 ± 0.016
	13	AUC	0.714	0.684 ± 0.006	0.719 ± 0.018
PadChest	61	AUC	0.715	0.702 ± 0.011	0.741 ± 0.005
VinDr-CXR	20	AUC	0.774	0.771 ± 0.024	0.831 ± 0.009

Table 3. Zero-shot classification performance of BioViL-T, CheXzero and our single best model Our_{single,best} (SLIP w/ ours) on the four different datasets (mean ± std). The best performance is in bold. The dataset setting is the same as in Table 1. All AUCs are mean values among diseases.

	mean AUC	Mean F1	Mean MCC
Our _{ensemble,best}	0.900 (0.868, 0.929)	0.638 (0.566, 0.707)	0.552 (0.468, 0.633)
CheXzero _{ensemble}	0.824 (0.777, 0.866) ^a	0.573 (0.493, 0.652) ^a	0.432 (0.339, 0.528) ^a
BioViL	0.812 (0.762, 0.857) ^a	0.558 (0.480, 0.634) ^a	0.423 (0.331, 0.511) ^a
Xplainer ^b	0.864 (0.823, 0.901) ^a	0.607 (0.531, 0.683) ^a	0.493 (0.403, 0.585) ^a

Table 4. Zero-shot classification performance of CheXzero, BioViL-T, Xplainer, and our best ensemble model, Our_{ensemble,best} (UniCLIP_{ensemble} w/ ours), on the CheXpert test set using bootstrap for five competition pathologies (Atelectasis, Cardiomegaly, Consolidation, Edema, Pleural Effusion). The numbers in parentheses indicate the 95% confidence intervals (CI). ^ap-value < 0.001, Our_{ensemble,best} wins significantly. ^bUse external observation descriptions.

	Open-i		PadChest	
	Sentence-level	Report-level	Sentence-level	Report-level
CLIP	0.275 \pm 0.053	0.407 \pm 0.007	0.102 \pm 0.099	0.135 \pm 0.111
CLIP w/ours	0.658 \pm 0.005	0.693 \pm 0.005	0.572 \pm 0.021	0.579 \pm 0.015
SLIP	0.163 \pm 0.021	0.287 \pm 0.031	0.007 \pm 0.022	0.018 \pm 0.014
SLIP w/ours	0.434 \pm 0.034	0.489 \pm 0.035	0.512 \pm 0.008	0.500 \pm 0.009
UniCLIP	0.209 \pm 0.013	0.318 \pm 0.016	0.096 \pm 0.010	0.118 \pm 0.011
UniCLIP w/ours	0.451 \pm 0.038	0.543 \pm 0.024	0.396 \pm 0.060	0.418 \pm 0.068
CheXzero	0.319 \pm 0.015	0.387 \pm 0.015	0.232 \pm 0.079	0.258 \pm 0.081
BioViL-T	0.628	0.315	0.241	0.158

Table 5. Image-text similarity for Open-i and PadChest datasets (mean \pm std). We report both sentence-level similarity and report-level similarity for each dataset.

	Text aug	Relax loss	Atelectasis	Cardiomegaly	Consolidation	Edema	Pleural effusion	Avg. 5 AUC	Avg. total AUC
CLIP			0.828 \pm 0.016	0.845 \pm 0.012	0.895 \pm 0.007	0.861 \pm 0.016	0.878 \pm 0.020	0.861 \pm 0.002	0.787 \pm 0.044
		✓	0.858 \pm 0.009	0.815 \pm 0.013	0.889 \pm 0.023	0.875 \pm 0.022	0.890 \pm 0.006	0.865 \pm 0.002	0.794 \pm 0.045
	✓		0.864 \pm 0.004	0.867 \pm 0.008	0.904 \pm 0.015	0.903 \pm 0.003	0.877 \pm 0.021	0.883 \pm 0.005	0.820 \pm 0.001
	✓	✓	0.859 \pm 0.006	0.840 \pm 0.016	0.913 \pm 0.010	0.881 \pm 0.009	0.869 \pm 0.012	0.872 \pm 0.005	0.824 \pm 0.003
SLIP			0.760 \pm 0.046	0.788 \pm 0.008	0.877 \pm 0.028	0.847 \pm 0.021	0.902 \pm 0.010	0.835 \pm 0.010	0.791 \pm 0.015
		✓	0.826 \pm 0.010	0.828 \pm 0.010	0.899 \pm 0.006	0.873 \pm 0.013	0.899 \pm 0.010	0.865 \pm 0.005	0.828 \pm 0.003
	✓		0.830 \pm 0.022	0.837 \pm 0.021	0.864 \pm 0.042	0.899 \pm 0.008	0.876 \pm 0.013	0.861 \pm 0.004	0.800 \pm 0.015
	✓	✓	0.845 \pm 0.014	0.855 \pm 0.018	0.904 \pm 0.014	0.905 \pm 0.016	0.868 \pm 0.009	0.875 \pm 0.006	0.819 \pm 0.028
UniCLIP			0.774 \pm 0.060	0.833 \pm 0.012	0.869 \pm 0.016	0.856 \pm 0.033	0.882 \pm 0.020	0.843 \pm 0.010	0.750 \pm 0.016
		✓	0.840 \pm 0.009	0.818 \pm 0.021	0.870 \pm 0.012	0.869 \pm 0.014	0.897 \pm 0.021	0.859 \pm 0.008	0.808 \pm 0.023
	✓		0.860 \pm 0.012	0.862 \pm 0.010	0.900 \pm 0.019	0.879 \pm 0.005	0.887 \pm 0.012	0.877 \pm 0.009	0.790 \pm 0.020
	✓	✓	0.870 \pm 0.007	0.844 \pm 0.007	0.911 \pm 0.002	0.886 \pm 0.014	0.882 \pm 0.017	0.878 \pm 0.001	0.825 \pm 0.028

Table 6. Ablation study of different components of our proposed method on the CheXpert validation set (mean \pm std). We report the zero-shot classification performance on three different CLIP-like frameworks. Best performance is in bold and second best is in underline for each framework. For the CheXpert dataset, the AUC for each of the five competition pathologies (Atelectasis, Cardiomegaly, Consolidation, Edema, Pleural Effusion), the average value of these five pathologies, and the total of 13 pathologies of this dataset are reported.

	$n = 1$	$n = 2$	$n = 3$	$n = 4$	$n = 5$
Avg. # of report	8433.86	538.40	106.20	25.24	1.03

Table 7. Average number of reports which contains same label combinations for CheXpert label. n is number of shared labels.

$E_{txt}(\mathbf{T}_{+,c})$, $E_{txt}(\mathbf{T}_{+,-}) \in \mathbb{R}^{d_T}$ (Fig. 3 (right)). d_I and d_T means embedding dimension of image encoder and text encoder, respectively.

$$\begin{aligned}
 s_{+,c} &= E_{img}(\mathbf{I}_{trg}) \cdot E_{txt}(\mathbf{T}_{+,c}), \\
 s_{-,c} &= E_{img}(\mathbf{I}_{trg}) \cdot E_{txt}(\mathbf{T}_{-,c}), \\
 prob_c &= \text{softmax}(s_{+,c}, s_{-,c}),
 \end{aligned} \tag{1}$$

where c indicates target pathology, $s_{+,c}$ and $s_{-,c}$ are the cosine similarity of positive and negative prompt, respectively.

Random sentence sampling

Unlike the general domain, the medical domain suffers from a scarcity of large-scale, high-quality datasets due to the laborious nature of obtaining expert annotation. Text augmentation is the most widely used solution to address this data shortage. However, the specific nature of medical reports presents unique challenges. Medical reports consist of formal and dense sentences with meaningful content crucial for diagnosis. Traditional

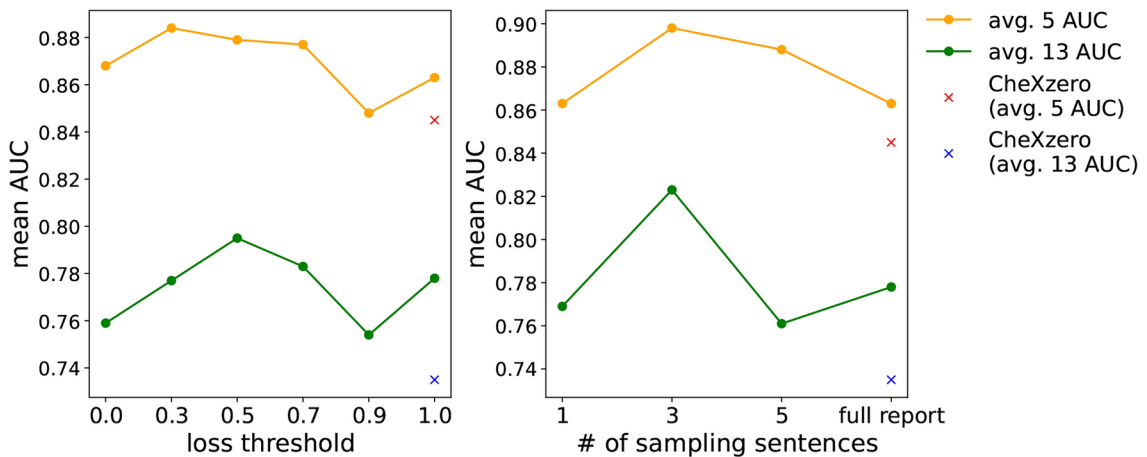


Figure 4. Effect of relaxing threshold (left) and number of sampling sentences per report (right). Both evaluate the zero-shot classification performance on the CheXpert validation set.

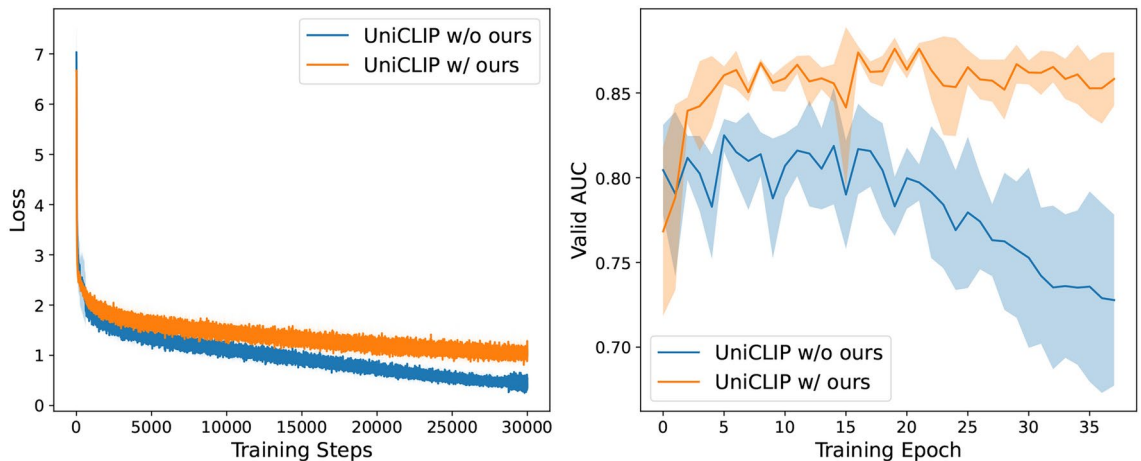


Figure 5. Training Loss (left) and AUROC on the CheXpert validation set (right) for two configurations: UniCLIP without our method ('w/o ours') and UniCLIP with our method ('w/ ours').

augmentation techniques, such as token-level deletion or swapping, risk altering the clinical accuracy by potentially removing essential medical terms (Fig. 2 (left)).

In addition, given that medical reports resemble lists more than narrative texts, where each sentence corresponds to a specific finding or label, they require specialized processing methods that focus on enhancing embeddings for individual labels, not just the entire report. To address this, we propose a simple, yet effective, unsupervised text processing method to tackle this issue. We randomly sub-sample n sentences from the report for every sample and feed them into the contrastive learning framework. Assuming the report contains m sentences, the image can be matched to mC_n positive samples through stochastic sub-sampling. This process enables the model to learn the rich semantics of each sentence, rather than training with just a single positive pair.

Loss for relaxed image-text agreement

CLIP¹¹ jointly trains an image encoder and a text encoder to predict the correct pairings of image-text pairs. Given a batch of N image-text pairs, CLIP maximizes the similarity between N positive pairs while minimizing the similarity between $N^2 - N$ negative pairs by the InfoNCE loss¹⁷, as follows.

$$\mathcal{L} = -\frac{1}{2N} \left(\sum_{i=1}^N \log \frac{\exp(\text{sim}(u_i, v_i)/\tau)}{\sum_{j=1}^N \exp(\text{sim}(u_i, v_j)/\tau)} + \sum_{i=1}^N \log \frac{\exp(\text{sim}(v_i, u_i)/\tau)}{\sum_{j=1}^N \exp(\text{sim}(v_i, u_j)/\tau)} \right) \quad (2)$$

where u, v are the normalized vectors from the image and text encoders and (u_i, v_i) is a positive pair. sim is a function to calculate the similarity between two vectors, and τ denotes the learnable temperature.

However, the CLIP objective function does not consider false-negative cases, which have similar semantics but are treated as negative pairs. Unfortunately, false-negative pairs (Fig. 1) are more likely to occur due to the fine-grained label scope of the medical domain compared to the general domain. Therefore, enforcing an increase in similarity only for positive pairs, despite the existence of false-negatives, may mislead the model. We argue that reducing the attraction between positive pairs can alleviate this problem. We propose the modified **sim** function that makes the model focus on perfectly negative pairs (images or reports from different patients with different semantics) instead of false-negative pairs by clipping the upper bound of the similarity function.

$$\text{sim}(u_i, v_j) = \begin{cases} \frac{1}{1+\exp(-\alpha(u_i \cdot v_j - t))}, & \text{if } i = j \text{ and } u_i \cdot v_j \geq t \\ u_i \cdot v_j / 2t, & \text{else if } i = j \text{ and } t > u_i \cdot v_j \geq 0 \\ u_i \cdot v_j, & \text{otherwise} \end{cases} \quad (3)$$

, where $u_i \cdot v_j$ denotes cosine similarity between two vectors, α a slope coefficient of the Sigmoid function. A threshold of t ($0 < t < 1$) is used to determine the level of attractiveness between positive pairs. With our modified similarity function, positive pairs with a similarity score $\text{sim}(u_i \cdot v_i) \geq t$ quickly reach a maximum similarity value (i.e., loss of those pairs becomes minimum). Note that we separately defined the second and third terms of (3) for the continuity of the sim function when $u_i \cdot v_i = 0$ and $u_i \cdot v_i = t$, ensuring stable backpropagation. Note that CLIP-like methods, such as SLIP and UniCLIP, utilize similarity between samples, despite differences in how they construct the positive set. Therefore, the **sim** function can be easily substituted for those losses.

Datasets

For model training, we use MIMIC-CXR¹⁸, a large public dataset, as the training set, and evaluate its performance on four different publicly available datasets: CheXpert¹³, Open-i¹⁹, PadChest²⁰, and VinDr-CXR²¹. Each dataset is described in detail below and the statistics for each are presented in Table 8.

MIMIC-CXR: MIMIC-CXR¹⁸ is a large-scale public database that includes 377,110 chest radiographs corresponding to 227,835 studies in free-text format. We used this dataset to fine-tune the CLIP frameworks. Since meaningful observations are mainly written in the “Findings” or “Impression” sections, we extract those two sections for each study (<https://github.com/MIT-LCP/mimic-cxr>). If the section is not extracted by the rule-based method, we use the last paragraph of those samples. All radiographs are used for fine-tuning regardless of view (AP, PA, and lateral).

CheXpert: CheXpert¹³ is a public dataset from Stanford Hospital, that includes 224,316 chest radiographs of 65,240 patients, annotated with 14 classes. The validation and test sets have 234 and 668 images, respectively. We use CheXpert’s validation set for model selection and the test set for evaluation. Since the test and validation sets of the CheXpert dataset are manually annotated by board-certified radiologists, we use the CheXpert validation set for model selection, following the approach used in CheXzero¹⁰. Specifically, we select the model based on the mean AUROC of the validation set across the five CheXpert competition tasks: Atelectasis, Cardiomegaly, Consolidation, Edema, and Pleural Effusion (<https://stanfordmlgroup.github.io/competitions/chexpert>). For evaluation, we use not only the above five tasks, but also all labels from the CheXpert test set, except for “no finding.” This exception is made since predicting all labels as zero is equivalent to a “no finding” label in a multi-label setting.

PadChest: The PadChest²⁰ is a public dataset provided by the Medical Imaging Databank of the Valencia Region. This dataset consists of more than 160,000 chest radiograph images of 67,000 patients from San Juan Hospital (Spain) from 2009 to 2017. PadChest is annotated with 174 different findings and 19 differential diagnoses. We used only 15,091 examples ($n = 15,091$) as a test set, which board-certified radiologists manually annotated. We used 61 radiographic findings with more than 100 samples in the test set. We use the PadChest test set to evaluate zero-shot classification performance and image-text alignment.

Open-i: Open-i collection²² is a service for abstract and image search by the National Library of Medicine (NLM). The Open-i chest radiograph dataset includes 7470 images and 3,955 reports provided by Indiana University Hospital. We select the “Finding” and “Impression” sections which contain essential information

		# of Images	# of Reports	# of classes in use
Fine-tuning	MIMIC-CXR ¹⁸	377,110	227,835	–
	CheXpert _{valid} ¹³	234	–	5/14
Evaluation	CheXpert _{test} ¹³	668	–	5, 13/14
	Open-i ³²	2,550	2,550	5, 13/14
	PadChest ²⁰	15,091	15,091	61/174
	VinDr-CXR ²¹	3,000	–	20/28

Table 8. The statistics of datasets.

associated with the X-ray images. We first select the image-text pair with frontal view images and filtered samples with a report length of 10 characters or more. We used a pre-processed dataset with 2,550 image-text pairs as our test set to evaluate image-text similarity and zero-shot classification. For reference, the data is labeled using the CheXpert labeler tool provided by the authors (<https://github.com/stanfordmlgroup/chexpert-labeler>)¹³.

VinDr-CXR: VinDr-CXR²¹ includes 18,000 images, 15,000 for the train set and 3,000 for the test set, collected from two major hospitals in Vietnam. A total of 17 board-certified radiologists annotated them with 28 labels consisting of 22 local abnormalities and 6 global suspected diseases. Each scan in the test set was labeled by consensus of 5 radiologists. We evaluate zero-shot classification for 20 labels with more than 20 samples within the test set.

Implementation details

In this paper, we fine-tune three CLIP-based frameworks, CLIP¹¹, SLIP²³ and UniCLIP²⁴ with and without our proposed methods to demonstrate their effectiveness. To evaluate the efficacy of our approach, we conducted comparisons against several recently proposed state-of-the-art, label-free methods, CheXzero¹⁰ and BioViL-T⁹. Additionally, we compared our method to Xplainer²⁵, which integrates external knowledge about target diagnoses with the BioViL framework. It is important to note that Xplainer requires additional descriptions for each target diagnosis, limiting its application to only the CheXpert dataset among our target test datasets. Our CLIP framework consists of ViT-B/16 and BERT_{base} without our proposed method, which might appear similar to the CheXzero configuration. However, CheXzero uses ViT-B/32 as an image encoder and BERT_{base} as a text encoder. The baseline “CheXzero” in this paper follows the original configuration for fair evaluation. In all settings, the dimensions for the image and text encoders, d_I and d_T , are consistently fixed at 768.

We utilized the BERT_{base} model²⁶ as our text encoder and the ViT-B/16²⁷ as our image encoder within three CLIP-based frameworks as described above (i.e., CLIP, SLIP, UniCLIP). For CLIP and UniCLIP, we initialize the model using the publicly available pre-trained weight provided by OpenAI (<https://github.com/openai/CLIP>). In the case of SLIP, we use the model checkpoint that was pre-trained with the YFCC-15M dataset²⁸ for initialization (<https://github.com/facebookresearch/SLIP>). Note that all baseline models, including CLIP, SLIP, and UniCLIP, have been fine-tuned following the methods outlined in their respective papers. The term “w/ ours” indicates models that were fine-tuned using their original methods, but with the addition of our strategy, which includes random sentence sampling and loss relaxation. For BioViL-T and Xplainer, we used the officially released checkpoints from Hugging Face (<https://huggingface.co/microsoft/BiomedVLP-BioViL-T>), as neither framework provided training scripts. For CheXzero, we retrained the model using our training hyperparameters and image augmentation settings, as we found that our configuration achieved a higher CheXpert validation AUROC (0.870 vs. 0.864) than the original configuration.

In our text sampling approach, we randomly sampled three sentences ($n = 3$) from each report. The relaxation loss threshold was set at $t = 0.5$, and the slope coefficient α was fixed at 10. For image augmentation, we apply random affine transformations with the following hyperparameters, rotations: $(-20, 20)$, resize crop ratio: $(0.9, 1.1)$, horizontal flip: true/false, color jitter (brightness and contrast): $(0.5, 2)$. These augmentations are based on the UniCLIP setting²⁴, but we reduced their intensity to avoid cropping important parts of the CXR. While CLIP and SLIP primarily use random square cropping from resized images during the pre-training phase, we adopted the random affine image augmentation method for fine-tuning since we found that these augmentations improved the CheXpert validation AUROC. We set the image resolution at 224×224 . We implement the entire model in PyTorch²⁹ and train the network over 50 epochs with a batch size of 1024 across 8 GPUs on the A100 server (NVIDIA Corp.). We use the Adam optimizer³⁰ with an initial learning rate 1×10^{-4} and decay the learning rate using a cosine scheduler with a warm-up for 100 iterations³¹. We conducted a hyperparameter sweep over batch size and learning rate using the CheXpert validation dataset. We first selected the hyperparameters for CLIP fine-tuning without our method, then added our method while keeping all other parameters unchanged. This demonstrates the advantage of our method, as it can improve model performance simply by adding it without altering any other parameters. To ensure robustness, we repeat all experiments three times with different random seeds and report the mean and standard deviation for the single model results. The ensemble results are derived from the average predictions of these three models. Since standard deviations cannot be reported for the ensemble model, we include confidence intervals and p-values to demonstrate statistical significance. These statistics are calculated using a non-parametric bootstrap method, as detailed in the revised version of CheXzero. Specifically, we generated 1,000 bootstrap samples of size n (equal to the size of the original dataset) with replacement.

Evaluation tasks

Zero-shot classification

We perform a zero-shot multi-label image classification on four datasets; CheXpert, PadChest, Open-i, and VinDr-CXR. For CheXpert and Open-i, we use all 13 pathologies. For PadChest, we use 61 labels out of a total of 193, each of which has more than 100 patients. Finally, VinDr-CXR is evaluated with 20 of 28 labels that include more than 20 patients. The macro AUROC (Area under the ROC curve) for multi-label is used as an evaluation metric. We calculated the binary AUROC for each label separately and then computed the macro average.

Image-text alignment

In a medical report, each sentence generally contains different label information. Therefore, measuring image-text alignment not only at the report level but also at the sentence level can indicate how the learned embedding contains semantics for each label. We calculate the cosine similarity between image embedding and report embedding for each X-ray-Report pair for report-level evaluation. We measure sentence-level alignment by

calculating the average similarity between the image and the sentence embedding for all sentences in a given report.

Results

Zero-shot classification

We empirically validate that our fine-tuning strategies consistently improve the zero-shot classification performance on 4 independent datasets collected from four different countries: CheXpert¹³, Open-i¹⁹, PadChest²⁰, and VinDR-CXR²¹. CheXpert and Open-i are evaluated on the same CheXpert 13 labels. PadChest and VinDR-CXR are evaluated on 61 labels and 20 labels, respectively. A list of all labels used for evaluation is in the Table 9. Please refer to the “Datasets” section in the Method for detailed information about those evaluation datasets.

To analyze the effect of our proposed method, we experimented with three different CLIP-like frameworks: CLIP¹¹, SLIP²³ and UniCLIP²⁴. In Table 1, we demonstrate the effectiveness and generalizability of our method by showing consistent results in different labels and data distributions. We show significant improvements compared to baseline performance (i.e., using our fine-tuning strategy) in the three CLIP-like frameworks and four datasets. We observe an average 5.77% increase in AUROC in zero-shot classification. For details, the CLIP baseline improved by 3.4% increase, SLIP by 6.86%, and UniCLIP by 7.05%. These results mean that our method successfully embeds the multi-pathology feature, reflecting the nature of the medical data well. In addition, we also show that using an ensemble of selected models brings significant improvements in all cases (Table 2). We also show that the model can perform pathology classification performance comparable to that of board certified radiologists using our method in Table 2. Furthermore, in the case of SLIP and UniCLIP, they outperform the expert-level by adopting our strategy with ensembles.

We compare our best single results, achieved with SLIP, to the current state-of-the-art models in Table 3. Our model consistently outperforms CheXzero across all datasets and surpasses BioViL-T in most metrics. The only exception is the total AUROC for the CheXpert dataset, where our model’s performance aligns with BioViL-T. These findings confirm that our approach has the potential to deliver superior performance relative to existing state-of-the-art models. In Table 4, we present the mean performance of our best ensemble model (UniCLIP_{ensemble} w/ ours) alongside the current state-of-the-art models, detailing their performance differences with a 95% confidence interval (CI). Our model also significantly exceeds the performance of existing models on all reported metrics for the zero-shot classification of the CheXpert dataset.

Image-text alignment

We analyze how our method enhances the semantic representation quality of the model embeddings by improving image-text alignment at both the sentence and the report levels. To elaborate, “sentence-level” alignment targets individual sentences within a report, whereas “report-level” alignment considers the report’s entire content. Given that each sentence in a medical report often presents unique clinical findings, we hypothesize that sentence-level alignment assessment provides insights into the model’s ability to handle detailed multi-label information.

The effectiveness of our approach is evidenced by significant improvements in model alignment at both the sentence and report levels, as shown in Table 5. Our method also narrows the disparity between these two levels of measurement. BioViL-T⁹, which employs sentence shuffling during text encoder pre-training, shows higher sentence-level similarity than the CLIP-base framework without our strategy. However, a significant gap in report-level similarity remains with these baselines. Our random text sampling prevents the model from overfitting to specific report sections. This approach not only enables the model to focus on crucial pathological information in individual sentences, but also enhances its ability to represent these insights in semantically rich report-level embeddings. One potential concern with our methodology is the possibility of losing critical information during sub-sampling of sentences. Our training strategy involves randomly sub-sampling three sentences per epoch over 50 epochs. Considering that each MIMIC-CXR report contains seven sentences on average, our method is expected to cover all sentences in most reports at least once. Evidence for this is the higher report-level and sentence-level similarity, even surpassing those trained with entire reports. Furthermore, the succinct and structured nature of medical reports makes our method particularly effective in bridging

	Names
CheXpert ¹³	Enlarged cardiomegaly, lung opacity, lung lesion, edema, consolidation, pneumonia, atelectasis, pneumothorax, pleural effusion, pleural other, fracture, support devices
Open-i ¹⁹	Enlarged cardiomegaly, lung opacity, lung lesion, edema, consolidation, pneumonia, atelectasis, pneumothorax, pleural effusion, pleural other, fracture, support devices
PadChest ²⁰	Air trapping, alveolar pattern, aortic atherosclerosis, aortic button enlargement, aortic elongation, apical pleural thickening, atelectasis, bronchiectasis, bronchovascular markings, bullas, calcified densities, calcified granuloma, callus rib fracture, cardiomegaly, consolidation, copd signs, costophrenic angle blunting, descendent aortic elongation, diaphragmatic eventration, dual chamber device, emphysema, fibrotic band, flattened diaphragm, goiter, granuloma, gynecomastia, heart insufficiency, hemidiaphragm elevation, hiatal hernia, hilar congestion, hilar enlargement, hyperinflated lung, increased density, infiltrates, interstitial pattern, kyphosis, laminar atelectasis, mammary prosthesis, metal, nipple shadow, nodule, osteopenia, osteosynthesis material, pacemaker, pleural effusion, pleural thickening, pneumonia, pseudonodule, pulmonary mass, sclerotic bone lesion, scoliosis, single chamber device, sternotomy, supra aortic elongation, suture material, tracheal shift, tuberculosis sequelae, vascular hilar enlargement, vertebral anterior compression, vertebral degenerative changes, volume loss
VinDr-CXR ²¹	Aortic enlargement, atelectasis, calcification, cardiomegaly, consolidation, ILD, infiltration, lung opacity, mediastinal shift, nodule/mass, pleural effusion, pleural thickening, pneumothorax, pulmonary fibrosis, rib fracture, other lesion, lung tumor, pneumonia, tuberculosis, other disease

Table 9. All labels used in this paper.

the domain gap across different datasets. Despite the PadChest reports being in Spanish and having a more significant data gap with our training dataset, MIMIC-CXR, our approach still shows notable performance improvements (Table 5).

Discussion

Our method is based on two factors: random sentence sampling within the report and loss relaxation to regularize image-text agreement. We analyze the effectiveness of the factors of our method by comparing the zero-shot pathology classification performance on the CheXpert validation set. In Table 6, we verify the benefits conferred by each component. While loss relaxation deals with potential false-negative cases, random sentence sampling directly enriches the diversity of the training data, encouraging the model to learn a more robust embedding.

Our experimental results, as presented in Table 6, indicate that performance is typically optimal when both strategies are employed. Hence, we suggest using both fine-tuning approaches as a standard solution. The degree of enhancement can vary depending on the pathology. For example, the performance of pleural effusion improved primarily with loss relaxation, while other pathologies benefited more from text sampling. Such disparities could arise from variations in how each pathology is described in reports and differences in the distribution of labels between data.

We determined the optimal hyperparameters n and t for our strategy by evaluating zero-shot classification performance with various settings, as shown in Fig. 4. Our hyperparameters are deciding number of sentences (n) to sample in a report and the threshold (t) for transforming cosine similarity during fine-tuning. Based on our observations, we set the sentence sampling hyperparameter to $n = 3$ and the loss relaxation hyperparameter to $t = 0.5$.

Sentence sampling may generate false-negative pairs if randomly extracted sentences unintentionally have the same labels. Table 7 shows that, on average, 8,433 reports share one label, 538 two labels, etc. From Table 7 and Fig. 4, we can conclude that sampling three sentences per report makes a great compromise between the number of false-negatives and the effectiveness of contrastive learning. Note that there still exists partial overlap between sampled sentences, but this is addressed by our loss relaxation.

In terms of computational load, our method, which includes text sampling and loss relaxation, can be directly applied to existing CLIP-based models without any changes to the model architecture. Therefore, the potential impact on computational load of our method is limited to random text selection and the loss computation process. These operations do not significantly impact the overall computational load, as they are lightweight and efficiently handled by modern deep learning frameworks. Consequently, the time efficiency of our method is equivalent to that of the base models when both are trained over the same number of epochs. To analyze the impact of our method on training efficiency, we provide training loss graphs and validation AUROC graphs for UniCLIP and UniCLIP with our method. As shown in Fig. 5, the difference in the speed of loss reduction is not substantial, indicating that our method does not significantly affect the overall training time needed for saturation. Additionally, UniCLIP w/ ours consistently achieves higher validation AUROC values compared to UniCLIP w/o ours. It reaches higher performance levels more rapidly and maintains stability throughout the training epochs. These results demonstrate that our methodology effectively improves the model performance without introducing significant computational overhead.

In this paper, we propose a simple yet effective fine-tuning strategy for medical image-text multi-modal learning. Our method consists of two ways, sentence sampling and loss relaxation, to reflect the multi-label nature of the medical image-text data. Our fine-tuning strategy improves zero-shot pathology classification performance in all three CLIP-based frameworks. Furthermore, our proposed method significantly outperformed board-certified radiologists without additional label information for two frameworks. Additionally, we validate the effect of our method through image-text alignment tasks on two radiography datasets. Although our model shows comparable, or sometimes superior performance compared to the expert level in pathology classification performance, it is difficult to determine whether the model's judgments are based on the location of the pathology. For future work, we plan to explore the medical multi-modal representation learning method that can consider these localized features.

Data availability

The datasets analyzed in this study are available on MIMIC-CXR (<https://physionet.org/content/mimic-cxr/2.0.0/>), <https://www.physionet.org/content/mimic-cxr-jpg/2.0.0/>), CheXpert (<https://stanfordmlgroup.github.io/competitions/chexpert/>), Open-i (<https://openi.nlm.nih.gov/>), PadChest (<https://bimcv.cipf.es/bimcv-projects/padchest/>), and VinDr-CXR (<https://physionet.org/content/vindr-cxr/1.0.0/>).

Received: 4 January 2024; Accepted: 19 September 2024

Published online: 05 October 2024

References

1. Gulshan, V. et al. Development and validation of a deep learning algorithm for detection of diabetic retinopathy in retinal fundus photographs. *JAMA* (2016).
2. Krause, J. et al. Grader variability and the importance of reference standards for evaluating machine learning models for diabetic retinopathy. *Ophthalmology* **125**, 1264–1272 (2018).
3. Esteva, A. et al. Dermatologist-level classification of skin cancer with deep neural networks. *Nature* **542**, 115–118 (2017).
4. Mustafa, B. et al. Supervised transfer learning at scale for medical imaging. arXiv preprint [arXiv:2101.05913](https://arxiv.org/abs/2101.05913) (2021).
5. Ke, A., Ellsworth, W., Banerjee, O., Ng, A. Y. & Rajpurkar, P. CheXtransfer: performance and parameter efficiency of imagnet models for chest x-ray interpretation. In *Proceedings of the Conference on Health, Inference, and Learning*, 116–124 (2021).
6. Azizi, S. et al. Big self-supervised models advance medical image classification. In *Proceedings of the IEEE/CVF International Conference on Computer Vision*, 3478–3488 (2021).

7. Zhang, Y., Jiang, H., Miura, Y., Manning, C. D. & Langlotz, C. P. Contrastive learning of medical visual representations from paired images and text. *arXiv preprint[SPACE]arXiv:2010.00747* (2020).
8. Huang, S.-C., Shen, L., Lungren, M. P. & Yeung, S. G. A multimodal global-local representation learning framework for label-efficient medical image recognition. In *2021 IEEE/CVF International Conference on Computer Vision (ICCV)*, 3922–3931 (2021).
9. Boecking, B. et al. Making the most of text semantics to improve biomedical vision–language processing. In *European conference on computer vision*, 1–21 (Springer, 2022).
10. Tiu, E. et al. Expert-level detection of pathologies from unannotated chest x-ray images via self-supervised learning. *Nat. Biomed. Eng.* 1–8 (2022).
11. Radford, A. et al. Learning transferable visual models from natural language supervision. In *International Conference on Machine Learning*, 8748–8763 (PMLR, 2021).
12. Wang, Z., Wu, Z., Agarwal, D., & Sun, J. Contrastive learning from unpaired medical images and text. In *EMNLP (Medclip)*, 2022).
13. Irvin, J. et al. Chexpert: A large chest radiograph dataset with uncertainty labels and expert comparison. In *Proceedings of the AAAI conference on artificial intelligence* (2019).
14. Bayer, M. et al. A survey on data augmentation for text classification. *ACM Comput. Surveys* (2022).
15. Abdollahi, M. et al. Ontology-guided data augmentation for medical document classification. In *Artificial Intelligence in Medicine* (2020).
16. Ramesh, A. et al. Zero-shot text-to-image generation. In *International Conference on Machine Learning*, 8821–8831 (PMLR, 2021).
17. Oord, A. V.D., Li, Y. & Vinyals, O. Representation learning with contrastive predictive coding. *arXiv preprint[SPACE]arXiv:1807.03748* (2018).
18. Johnson, A. E. et al. Mimic-cxr, a de-identified publicly available database of chest radiographs with free-text reports. *Sci. Data* 6, 1–8 (2019).
19. Demner-Fushman, D. et al. Preparing a collection of radiology examinations for distribution and retrieval. *J. Am. Med. Inf. Assoc. JAMIA* 23 (2015).
20. Bustos, A., Pertusa, A., Salinas, J.-M. & de la Iglesia-Vayá, M. Padchest: A large chest x-ray image dataset with multi-label annotated reports. *Med. Image Anal.* 66, 101797 (2020).
21. Nguyen, H. Q. et al. Vindr-cxr: An open dataset of chest x-rays with radiologist's annotations. *Sci. Data* 9, 1–7 (2022).
22. Demner-Fushman, D., Antani, S., Simpson, M. & Thoma, G. R. Design and development of a multimodal biomedical information retrieval system. *J. Comput. Sci. Eng.* 6, 168–177 (2012).
23. Mu, N., Kirillov, A., Wagner, D. & Xie, S. Slip: Self-supervision meets language-image pre-training. *arXiv preprint[SPACE]arXiv:2112.12750* (2021).
24. Lee, J. et al. Uniclip: Unified framework for contrastive language-image pre-training. *arXiv preprint[SPACE]arXiv:2209.13430* (2022).
25. Pellegrini, C. et al. Xplainer: From x-ray observations to explainable zero-shot diagnosis. *MICCAI* (2023).
26. Devlin, J. et al. BERT: Pre-training of deep bidirectional transformers for language understanding. In *Proceedings of the 2019 Conference of the North American Chapter of the Association for Computational Linguistics: Human Language Technologies, Volume 1 (Long and Short Papers)* (2019).
27. Dosovitskiy, A. et al. An image is worth 16x16 words: Transformers for image recognition at scale. In *International Conference on Learning Representations* (2021).
28. Thomee, B. et al. YFCC100M: The new data in multimedia research. *Commun. ACM* 59, 64–73 (2016).
29. Paszke, A. et al. Pytorch: An imperative style, high-performance deep learning library. In *NeurIPS* (2019).
30. Kingma, D. P. & Ba, J. A method for stochastic optimization. In *ICLR (Adam)*, 2015).
31. Loshchilov, I. & Hutter, F. Sgdr: Stochastic gradient descent with warm restarts. *arXiv preprint[SPACE]arXiv:1608.03983* (2016).
32. Ai, O. <https://github.com/openai/clip>.

Acknowledgements

This work was conducted during the internship at LG AI Research. This work was supported by the Institute of Information & Communications Technology Planning & Evaluation (IITP) grant (No.RS-2019-II190075), and the Korea Health Industry Development Institute (KHIDI) grants (No.HI21C1138, No.HR21C0198) funded by the Korea government (MSIT, MOHW).

Author contributions

J.J. and D.K.: Designed the methodology and analysis, processed the data, performed the experiments and analysis, and wrote the paper. S.K., H.L., K.B.: Provided resources and reviewed the manuscript. E.C.: Provided supervision, analysis, and reviewed and edited the manuscript.

Additional information

Correspondence and requests for materials should be addressed to E.C.

Reprints and permissions information is available at www.nature.com/reprints.

Publisher's note Springer Nature remains neutral with regard to jurisdictional claims in published maps and institutional affiliations.

Open Access This article is licensed under a Creative Commons Attribution-NonCommercial-NoDerivatives 4.0 International License, which permits any non-commercial use, sharing, distribution and reproduction in any medium or format, as long as you give appropriate credit to the original author(s) and the source, provide a link to the Creative Commons licence, and indicate if you modified the licensed material. You do not have permission under this licence to share adapted material derived from this article or parts of it. The images or other third party material in this article are included in the article's Creative Commons licence, unless indicated otherwise in a credit line to the material. If material is not included in the article's Creative Commons licence and your intended use is not permitted by statutory regulation or exceeds the permitted use, you will need to obtain permission directly from the copyright holder. To view a copy of this licence, visit <http://creativecommons.org/licenses/by-nc-nd/4.0/>.

© The Author(s) 2024